An Adaptive Multi-sensor Fusion for Intelligent Vehicle Localization

Hao Zhu, Yujian Qiu, Yongfu Li, Lyudmila Mihaylova, and Henry Leung, *Fellow, IEEE,*

***Abstract*—Localization is a basic technology for intelligent vehicle (IV), which is usually carried out by fusing multiple sensors. In order to achieve robust and accurate localization results, a novel adaptive multi-sensor fusion method is proposed. For each sensor, every measurement is identified by an indicator, which is used to recognize whether the measurement has the useful information to improve the localization performance. A robust localization model of IV is then developed by using variational Bayesian approach. Simulations and experiments using a real IV are used to demonstrate the potential and effectiveness of the proposed method.**

***Index Terms*—Localization, intelligent vehicle, sensor fusion, variational Bayesian.**

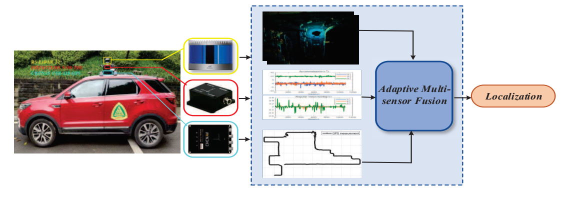

I. Introduction

INTELLIGENT vehicle (IV) is a hot topic for both industry and academia [1], while localization is a key component of an IV to provide robust and accurate estimates of its state [2]–[4].

An IV is equipped with many sensors, such as GPS, inertial measurement unit (IMU), light detection and ranging (Lidar), and cameras. The IMU gives a continuity solution of IV's state, its gyro suffers from time-varying biases and uncertain noises, and the accuracy of position and orientation estimates from IMU deteriorates over time. In [5], a Kalman filter (KF) incorporating a deep neural network is proposed to estimate the noise parameters for dead-reckoning. In [6], a prior on displacement distributions is obtained using a neural network with only IMU data. Then, the prior information is integrated with an extended KF (EKF) to estimate the state. Furthermore, sensor fusion is used to provide more accurate results in the literature [7], [8]. Many GPS/IMU systems have been developed for IV localization. The global position and velocity are provided by GPS, meanwhile, local position, orientation, and velocity are estimated from IMU. The GPS/IMU system can provide a robust localization solution in many scenarios. However, the GPS may have weak or even no signal in tunnels or parking lots. In the GPS-challenged environments or GPS-denied environments, the performance of GPS/IMU systems will be degraded. In [9], the state with unknown measurement loss is estimated by a Bayesian KF (BKF). However, the loss probability varies with the traffic, and the performance is degraded in such environments. Various localization approaches for IV in these environments have been developed. It can be roughly categorized into: map-based methods and simultaneous localization and mapping (SLAM) methods [10]–[14]. The map-based methods extract prior information about static environment to build high definition (HD) map in advance. The state of IV can then be obtained by matching with the existing HD map [15]. The SLAM methods provide the IV localization using online estimation and do not require prior information in advance [16]. In the literature, several SLAM methods have been proposed based on different sensors such as cameras, sonars, and Lidar [17]. The Lidar-based SLAM methods are found to have robust performance in most environments [16].

For Lidar-based SLAM, many methods have been developed. In [18], a real-time Lidar odometry and mapping (LOAM) method is proposed to estimate the state using edge and plane feature points. In [19], a lightweight and ground-optimized Lidar odometry and mapping (LEGO-LOAM) method is proposed to estimate the state of unmanned ground vehicles. Compared with LOAM, LEGO-LOAM is more efficient and reduces the drift in large-scale scenarios [19]. Furthermore, in order to achieve reliable and accurate state estimates, Lidar is considered in conjunction with IMU and GPS. In [20], a loosely-coupled method is proposed using Lidar and IMU date. IMU is used to give a motion prior for Lidar registration. In [21], a kinematic model of vehicle is developed to predict the ego-motion of vehicle and a robust localization method of vehicle is developed by unscented KF (UKF) method to

The work was supported in part by National Natural Science Foundation of China under Grant No. 62073052, No. U1964202, by the Natural Science Foundation of Chongqing under Grant No. cstc2021jcyj-msxmX0373, No. CSTB2023TIAD-STX0016, and by the Scientific and Technological Research Program of Chongqing Municipal Education Commission under Grant No. KJZD-K202200603.

Hao Zhu, Yujian Qiu, and Yongfu Li are with the Department of Automation, Chongqing University of Posts and Telecommunications, Chongqing 400065, China (e-mail: zhuhao@cqupt.edu.cn)

Lyudmila Mihaylova is with the Department of Automatic Control and Systems Engineering, The University of Sheffield, Sheffield S13JD, U.K.

Henry Leung is with the Department of Electrical and Computer Engineering, University of Calgary, Calgary AB T2N 1N4, Canada

fuse Lidar and IMU. In [22], the attitude of land vehicle is estimated using a velocity constraint for GPS/IMU. In [23], a variational Bayesian (VB) algorithm and switching KF are integrated to localize an IV using GPS and Lidar data. In [24], a robust Lidar-Inertial odometry, which is called Fast-LIO2, is proposed to localize an IV using an iterated KF. In [25], the ego-motion of IV is estimated by fusing Lidar and IMU using an iterated error-state KF.

All aforementioned methods directly fuse the measurements of all sensors to localize an IV. Since IV in extreme and unknown environments, such as tunnels. The environments have long and homogeneous structures, geometric features are scarce. As a result, the IV's motion is usually underestimated [26]. Therefore, the sensor measurement is not the true IV state information. In this article, a robust VB adaptive sensor fusion (VBASF) approach is developed to localize IV. In the proposed VBASF method, an indicator is introduced to each measurement for each sensor. The indicator follows a Bernoulli distribution and identifies whether the measurement is a state observation or an outlier. The problem of localization of IV is solved by the VB technique. The contributions are as follows:

1) Different from traditional fusion strategy [24], [25], which directly fuses all sensor measurements to estimate the IV's state, we propose in this paper to fuse only useful sensor measurements.

2) Lidar, IMU, and GPS measurements are transformed as linear functions of the IV states. A robust localization model is then constructed.

3) Experiments on real IV are carried out. The experimental results show the potential and effectiveness of the proposed VBASF method.

In Section II, the problem formulation is presented. In Section III, the proposed VBASF method is developed. The potential and effectiveness of the proposed VBASF method is verified in Section IV. Conclusion is provided in Section V.

II. Problem formulation

In this section, the localization of IV using IMU, GPS, and Lidar is formulated. Let $\mathbf{x}_t = \begin{bmatrix} (\mathbf{p}_t)^{\mathrm{T}} & (\boldsymbol{\varphi}_t)^{\mathrm{T}} & (\mathbf{v}_t)^{\mathrm{T}} & (\mathbf{w}_t)^{\mathrm{T}} \end{bmatrix}^{\mathrm{T}} \in \mathbb{R}^{12}$ denote the state of IV at time t, where $\mathbf{p}_t = \begin{bmatrix} p_t^x & p_t^y & p_t^z \end{bmatrix}^{\mathrm{T}}$ and $\boldsymbol{\varphi}_t = \begin{bmatrix} \theta_t & \psi_t & \phi_t \end{bmatrix}^{\mathrm{T}}$ are the position and orientation, respectively, p_t^x, p_t^y, and p_t^z are the positions of IV in the direction x, y, and z, respectively, θ_t, ψ_t, and ϕ_t are the pitch angle, yaw angle, and roll angle, respectively, $\mathbf{v}_t = \begin{bmatrix} v_t^x & v_t^y & v_t^z \end{bmatrix}^{\mathrm{T}}$ and $\mathbf{w}_t = \begin{bmatrix} w_t^x & w_t^y & w_t^z \end{bmatrix}^{\mathrm{T}}$ are the linear and angular velocity, respectively, v_t^x, v_t^y, and v_t^z are the linear velocity of IV in the direction x, y, and z, respectively, w_t^x, w_t^y, and w_t^z are angular velocity of IV in the pitch, yaw, and roll, respectively. The state of IV can be given as

$$\hat{\mathbf{x}}_{t|t-1} = f(\mathbf{x}_{t-1}, \Delta t) = \begin{bmatrix} \mathbf{p}_{t-1} + \mathbf{H}(\boldsymbol{\varphi}_{t-1})\mathbf{v}_{t-1}\Delta t \\ \boldsymbol{\varphi}_{t-1} + \mathbf{J}(\boldsymbol{\varphi}_{t-1})\mathbf{w}_{t-1}\Delta t \\ \mathbf{v}_{t-1} \\ \mathbf{w}_{t-1} \end{bmatrix} + \mathbf{q}_t \tag{1}$$

where $f(\mathbf{x}_{t-1})$ denotes the state transition function, $\mathbf{H}(\boldsymbol{\varphi}_{t-1})$ is the rotation matrix, $\mathbf{J}(\boldsymbol{\varphi}_{t-1})$ is the Jacobian matrix mapping the angular velocities to the Euler angles derivative, and Δt is the sample time step of the prediction stage, and $\mathbf{q}_t$ denotes the process noise with covariance matrix $\mathbf{Q}$.

The GPS provides the position measurement of IV,

$$\mathbf{g}_t = \mathbf{C}_1\mathbf{x}_t + \mathbf{e}_t^1 \tag{2}$$

where $\mathbf{g}_t$ denotes the GPS receivers position of IV, $\mathbf{C}_1 \in \mathbb{R}^{3\times 12}$ is given as

$$\mathbf{C}_1 = \begin{bmatrix} 1 & 0 & 0 & \mathbf{0}_{1\times 9} \\ 0 & 1 & 0 & \mathbf{0}_{1\times 9} \\ 0 & 0 & 1 & \mathbf{0}_{1\times 9} \end{bmatrix} \tag{3}$$

and $\mathbf{e}_t^1$ follows Gaussian distribution with mean zero and covariance $\mathbf{R}_1$.

The IMU gives the measurement of the angular velocity of IV, that is,

$$\mathbf{m}_t = \mathbf{C}_2\mathbf{x}_t + \mathbf{e}_t^2 \tag{4}$$

where $\mathbf{m}_t$ denotes the IMU measurement of IV's angular velocity, $\mathbf{C}_2 \in \mathbb{R}^{3\times 12}$ is given as

$$\mathbf{C}_2 = \begin{bmatrix} \mathbf{0}_{1\times 9} & 1 & 0 & 0 \\ \mathbf{0}_{1\times 9} & 0 & 1 & 0 \\ \mathbf{0}_{1\times 9} & 0 & 0 & 1 \end{bmatrix} \tag{5}$$

and $\mathbf{e}_t^2$ is white Gaussian noise with covariance $\mathbf{R}_2$.

The position variation $\Delta\mathbf{p}_t$ and orientation variation $\Delta\boldsymbol{\varphi}_t$ are provided by the Lidar odometry. It can be computed from the current and last measurements from Lidar by the traditional iterative closest point (ICP) point set registration method [27]. The measurements of linear and angular velocities are defined as

$$\mathbf{L}_t = \begin{bmatrix} \mathbf{v}_t^l \\ \mathbf{w}_t^l \end{bmatrix} = \begin{bmatrix} \mathbf{H}(\boldsymbol{\varphi}_{t-1})^{\mathbf{T}} & \mathbf{0} \\ \mathbf{0} & \mathbf{J}(\boldsymbol{\varphi}_{t-1})^{-1} \end{bmatrix} \begin{bmatrix} \Delta\mathbf{p}_t \\ \Delta\boldsymbol{\varphi}_t \end{bmatrix} \frac{1}{\Delta t} \tag{6}$$

where $\mathbf{L}_t = \begin{bmatrix} \mathbf{v}_t^l \\ \mathbf{w}_t^l \end{bmatrix}$ denotes the measurements of linear and angular velocities from Lidar at time t and Δt denotes the time interval. Therefore, the measurement function from Lidar can be given as

$$\mathbf{L}_t = \mathbf{C}_3\mathbf{x}_t + \mathbf{e}_t^3 \tag{7}$$

where $\mathbf{C}_3 \in \mathbb{R}^{6\times 12}$ is given as

$$\mathbf{C}_3 = \begin{bmatrix} \mathbf{0}_{1\times 6} & 1 & 0 & 0 & 0 & 0 & 0 \\ \mathbf{0}_{1\times 6} & 0 & 1 & 0 & 0 & 0 & 0 \\ \mathbf{0}_{1\times 6} & 0 & 0 & 1 & 0 & 0 & 0 \\ \mathbf{0}_{1\times 6} & 0 & 0 & 0 & 1 & 0 & 0 \\ \mathbf{0}_{1\times 6} & 0 & 0 & 0 & 0 & 1 & 0 \\ \mathbf{0}_{1\times 6} & 0 & 0 & 0 & 0 & 0 & 1 \end{bmatrix} \tag{8}$$

and $\mathbf{e}_t^3$ is white Gaussian noise with covariance $\mathbf{R}_3$.

From (2), (4), and (7), we have

$$p(\mathbf{g}_t \,|\mathbf{x}_t) = \mathcal{N}(\mathbf{g}_t; \mathbf{C}_1\mathbf{x}_t, \mathbf{R}_1) \tag{9}$$

$$p(\mathbf{m}_t \,|\mathbf{x}_t) = \mathcal{N}(\mathbf{m}_t; \mathbf{C}_2\mathbf{x}_t, \mathbf{R}_2) \tag{10}$$

$$p(\mathbf{L}_t \,|\mathbf{x}_t) = \mathcal{N}(\mathbf{L}_t; \mathbf{C}_3\mathbf{x}_t, \mathbf{R}_3) \tag{11}$$

where $\mathcal{N}(.)$ denotes the Gaussian distribution.

In a complex traffic environment, not all sensor measurements contain useful information, for example, GPS signal is not available in a tunnel, meanwhile, the motion of IV by Lidar-based point set registration methods is usually underestimated with only a few geometric features. To obtain a robust IV's motion, a novel multi-sensor fusion is developed. In the proposed method, a Bernoulli variable is proposed to identify whether the measurement is a state observation or an outlier. The measurement likelihood conditional on its Bernoulli random variable and IV's state can be expressed as

$$p(\mathbf{g}_t\,|\mathbf{x}_t\,) = \mathcal{N}(\mathbf{g}_t; \mathbf{C}_1\mathbf{x}_t, \mathbf{R}_1)^{\lambda_t}\mathcal{N}(\mathbf{g}_t; 0, \mathbf{R}_1)^{1-\lambda_t} \tag{12}$$

$$p(\mathbf{m}_t\,|\mathbf{x}_t\,) = \mathcal{N}(\mathbf{m}_t; \mathbf{C}_2\mathbf{x}_t, \mathbf{R}_2)^{\varepsilon_t}\mathcal{N}(\mathbf{m}_t; 0, \mathbf{R}_2)^{1-\varepsilon_t} \tag{13}$$

$$p(\mathbf{L}_t\,|\mathbf{x}_t\,) = \mathcal{N}(\mathbf{L}_t; \mathbf{C}_3\mathbf{x}_t, \mathbf{R}_3)^{\delta_t}\mathcal{N}(\mathbf{L}_t; 0, \mathbf{R}_3)^{1-\delta_t} \tag{14}$$

λ_t, ε_t, and δ_t are Bernoulli random variables, i.e., $\lambda_t \in \{0,1\}$, $\varepsilon_t \in \{0,1\}$, and $\delta_t \in \{0,1\}$. $\lambda_t = 1$, $\varepsilon_t = 1$, and $\delta_t = 1$ indicate that the $\mathbf{g}_t$, $\mathbf{m}_t$, and $\mathbf{L}_t$ are true state measurements, otherwise, $\lambda_t = 0$, $\varepsilon_t = 0$, and $\delta_t = 0$ refer to outliers. Then, the priors on the λ_t, ε_t, and δ_t can be formulated as

$$p(\lambda_t\,|\pi_t\,) = (\pi_t)^{\lambda_t}(1-\pi_t)^{(1-\lambda_t)} \tag{15}$$

$$p(\pi_t) = \mathrm{Be}(\pi_t; a_0, b_0) \tag{16}$$

$$p(\varepsilon_t\,|\alpha_t\,) = (\alpha_t)^{\varepsilon_t}(1-\alpha_t)^{(1-\varepsilon_t)} \tag{17}$$

$$p(\alpha_t) = \mathrm{Be}(\alpha_t; h_0, d_0) \tag{18}$$

$$p(\delta_t\,|\beta_t\,) = (\beta_t)^{\delta_t}(1-\beta_t)^{(1-\delta_t)} \tag{19}$$

$$p(\beta_t) = \mathrm{Be}(\beta_t; e_0, f_0) \tag{20}$$

where $\mathrm{Be}(.)$ denotes a Beta distribution, π_t, α_t, and β_t denote the probability of true state measurements of GPS, IMU, and Lidar, respectively, a_0, b_0, h_0, d_0, e_0, and f_0 denote the prior parameters.

The one-step predicted state is formulated as

$$p(\mathbf{x}_t\,|\mathbf{g}_{1:t-1}, \mathbf{m}_{1:t-1}, \mathbf{L}_{1:t-1}\,) = \mathcal{N}(\mathbf{x}_t; \hat{\mathbf{x}}_{t|t-1}, \mathbf{P}_{t|t-1}) \tag{21}$$

where $\hat{\mathbf{x}}_{t|t-1}$ and $\mathbf{P}_{t|t-1}$ denote the one-step predicted mean vector and covariance matrix estimates at time t, respectively, we have

$$\hat{\mathbf{x}}_{t|t-1} = f(\mathbf{x}_{t-1}) \tag{22}$$

$$\mathbf{P}_{t|t-1} = \mathbf{F}_{t-1}\mathbf{P}_{t-1|t-1}(\mathbf{F}_{t-1})^{\mathrm{T}} + \mathbf{Q} \tag{23}$$

where $\mathbf{F}_{t-1} = \partial f(\mathbf{x})/\partial \mathbf{x}|_{\mathbf{x}=\mathbf{x}_{t-1}}$, $\mathbf{x}_{t-1}$ and $\mathbf{P}_{t-1|t-1}$ denote the state mean vector and covariance matrix estimates of IV at time t-1, respectively.

III. VBASF METHOD

VB algorithm is proposed to estimate the Ψ_t in this section, where Ψ_t denotes the IV's state and parameters, i.e., $\Psi_t = \{\mathbf{x}_t, \lambda_t, \pi_t, \varepsilon_t, \alpha_t, \delta_t, \beta_t\}$. From VB method [28], [29],

$$\log q(\theta) = \mathrm{E}_{\Psi_t{}^{(-\theta)}}[\log p(\mathbf{g}_{1:t}, \mathbf{m}_{1:t}, \mathbf{L}_{1:t}, \Psi_t)] + c_\theta \tag{24}$$

where $\mathrm{E}[\,\cdot\,]$ is expectation, $\Psi_t{}^{(-\theta)} \cup \theta = \Psi_t$, θ means an item of Ψ_t, c_θ is a constant with respect to θ. The probability density function (PDF) $q(\theta)$ is computed as $q^{(j+1)}(\theta)$ using $q^{(j)}(\Psi_t{}^{(-\theta)})$ at the $j+1$th iteration [28]. Then, the PDF $p(\mathbf{g}_{1:t}, \mathbf{m}_{1:t}, \mathbf{L}_{1:t}, \Psi_t)$ is

$$\begin{aligned} & p(\mathbf{g}_{1:t}, \mathbf{m}_{1:t}, \mathbf{L}_{1:t}\,|\Psi_t\,) \\ = \; & \mathcal{N}(\mathbf{g}_t; \mathbf{C}_1\mathbf{x}_t, \mathbf{R}_1)^{\lambda_t}\mathcal{N}(\mathbf{g}_t; 0, \mathbf{R}_1)^{1-\lambda_t} \\ \times \; & \mathcal{N}(\mathbf{m}_t; \mathbf{C}_2\mathbf{x}_t, \mathbf{R}_2)^{\varepsilon_t}\mathcal{N}(\mathbf{m}_t; 0, \mathbf{R}_2)^{1-\varepsilon_t} \\ \times \; & \mathcal{N}(\mathbf{L}_t; \mathbf{C}_3\mathbf{x}_t, \mathbf{R}_3)^{\delta_t}\mathcal{N}(\mathbf{L}_t; 0, \mathbf{R}_3)^{1-\delta_t} \\ \times \; & \mathcal{N}(\mathbf{x}_t; \hat{\mathbf{x}}_{t|t-1}, \hat{\mathbf{P}}_{t|t-1}) \\ \times \; & (\pi_t)^{\lambda_t}(1-\pi_t)^{(1-\lambda_t)}(\alpha_t)^{\varepsilon_t}(1-\alpha_t)^{(1-\varepsilon_t)} \\ \times \; & (\beta_t)^{\delta_t}(1-\beta_t)^{(1-\delta_t)}\mathrm{Be}(\pi_t; a_0, b_0) \\ \times \; & \mathrm{Be}(\alpha_t; h_0, d_0)\mathrm{Be}(\beta_t; e_0, f_0) \\ \times \; & p(\mathbf{g}_{1:t-1})p(\mathbf{m}_{1:t-1})p(\mathbf{L}_{1:t-1}) \end{aligned} \tag{25}$$

Let $\theta = \mathbf{x}_t$ and from (24), we obtain

$$\begin{aligned} & \log q^{(j+1)}(\mathbf{x}_t) \\ \propto \; & -0.5\mathrm{E}^{(j)}[\lambda_t](\mathbf{g}_t - \mathbf{C}_1\mathbf{x}_t)^{\mathrm{T}}(\mathbf{R}_1)^{-1}(\mathbf{g}_t - \mathbf{C}_1\mathbf{x}_t) \\ & -0.5\mathrm{E}^{(j)}[\varepsilon_t](\mathbf{m}_t - \mathbf{C}_2\mathbf{x}_t)^{\mathrm{T}}(\mathbf{R}_2)^{-1}(\mathbf{m}_t - \mathbf{C}_2\mathbf{x}_t) \\ & -0.5\mathrm{E}^{(j)}[\delta_t](\mathbf{L}_t - \mathbf{C}_3\mathbf{x}_t)^{\mathrm{T}}(\mathbf{R}_3)^{-1}(\mathbf{L}_t - \mathbf{C}_3\mathbf{x}_t) \\ & -0.5(\mathbf{x}_t - \hat{\mathbf{x}}_{t|t-1})^{\mathrm{T}}(\mathbf{P}_{t|t-1})^{-1}(\mathbf{x}_t - \hat{\mathbf{x}}_{t|t-1}) + c_{\mathbf{x}_t} \\ \propto \; & -0.5(\mathbf{y}_t - \bar{\mathbf{C}}\mathbf{x}_t)^{\mathrm{T}}(\bar{\mathbf{R}}_t^{(j)})^{-1}(\mathbf{y}_t - \bar{\mathbf{C}}\mathbf{x}_t) \\ & -0.5(\mathbf{x}_t - \hat{\mathbf{x}}_{t|t-1})^{\mathrm{T}}(\hat{\mathbf{P}}_{t|t-1})^{-1}(\mathbf{x}_t - \hat{\mathbf{x}}_{t|t-1}) + c_{\mathbf{x}_t} \end{aligned} \tag{26}$$

where $\mathbf{y}_t$, $\bar{\mathbf{C}}$, and $\bar{\mathbf{R}}_t^{(j)}$ are given as

$$\mathbf{y}_t = \begin{bmatrix} \mathbf{g}_t \\ \mathbf{m}_t \\ \mathbf{L}_t \end{bmatrix} \tag{27}$$

$$\bar{\mathbf{C}} = \begin{bmatrix} \mathbf{C}_1 & \mathbf{0} & \mathbf{0} \\ \mathbf{0} & \mathbf{C}_2 & \mathbf{0} \\ \mathbf{0} & \mathbf{0} & \mathbf{C}_3 \end{bmatrix} \tag{28}$$

$$\bar{\mathbf{R}}_t^{(j)} = \begin{bmatrix} \mathbf{R}_1/\mathrm{E}^{(j)}[\lambda_t] & \mathbf{0} & \mathbf{0} \\ \mathbf{0} & \mathbf{R}_2/\mathrm{E}^{(j)}[\varepsilon_t] & \mathbf{0} \\ \mathbf{0} & \mathbf{0} & \mathbf{R}_3/\mathrm{E}^{(j)}[\delta_t] \end{bmatrix} \tag{29}$$

Therefore, the IV's can be computed using EKF method.

$$\hat{\mathbf{x}}_{t|t}^{(j+1)} = \hat{\mathbf{x}}_{t|t-1}^{(j+1)} + \mathbf{K}_t^{(l+1)}(\mathbf{y}_t - \bar{\mathbf{C}}\hat{\mathbf{x}}_{t|t-1}^{(j+1)}) \tag{30}$$

$$\mathbf{P}_{t|t}^{(j+1)} = \mathbf{P}_{t|t-1}^{(j+1)} - \mathbf{K}_t^{(l+1)}\bar{\mathbf{C}}\mathbf{P}_{t|t-1}^{(j+1)} \tag{31}$$

$$\mathbf{K}_t^{(j+1)} = \mathbf{P}_{t|t-1}^{(j+1)}\bar{\mathbf{C}}^{\mathrm{T}}(\bar{\mathbf{C}}\mathbf{P}_{t|t-1}^{(j+1)}\bar{\mathbf{C}}^{\mathrm{T}} + \bar{\mathbf{R}}_t^{(j)})^{-1} \tag{32}$$

where $\hat{\hat{\mathbf{x}}}_{t|t}^{(j+1)}$ and $\mathbf{P}_{t|t}^{(j+1)}$ denote the posterior of IV's state mean and covariance estimates, respectively, $\mathbf{K}_t^{(j+1)}$denotes the Kalman gain.

Let $\theta = \lambda_t$ and from (24), we have

$$\begin{aligned}&\log q^{(j+1)}(\lambda_t)\\ \propto\ &-0.5\lambda_t \mathrm{Tr}(\Delta_t^{(j+1)}(\mathbf{R}_1)^{-1}) - 0.5(1-\lambda_t)\mathrm{Tr}(\mathbf{g}_t{\mathbf{g}_t}^{\mathrm{T}}(\mathbf{R}_1)^{-1})\\ &+\lambda_t \mathrm{E}^{(j)}[\log(\pi_t)] + (1-\lambda_t)\mathrm{E}^{(j)}[\log(1-\pi_t)] + c_{\lambda_t}\end{aligned} \tag{33}$$

where $\mathrm{Tr}(.)$ stands for the trace of matrix and $\Delta_t^{(j+1)}$ is

$$\begin{aligned}&\Delta_t^{(j+1)}\\ =\ &\mathrm{E}^{(j+1)}\left[(\mathbf{g}_t - \mathbf{C}_1\mathbf{x}_t)(\mathbf{g}_t - \mathbf{C}_1\mathbf{x}_t)^{\mathrm{T}}\right]\\ =\ &(\mathbf{g}_t - \mathbf{C}_1\hat{\mathbf{x}}_{t|t}^{(j+1)})(\mathbf{g}_t - \mathbf{C}_1\hat{\mathbf{x}}_{t|t}^{(j+1)})^{\mathrm{T}} + \mathbf{C}_1\mathbf{P}_{t|t}^{(j+1)}{\mathbf{C}_1}^{\mathrm{T}}\end{aligned} \tag{34}$$

$q^{(j+1)}(\lambda_t)$ is approximated by a Bernoulli distribution, we obtain

$$\begin{aligned}\mathrm{Pr}^{(j+1)}(\lambda_t = 1) = \ &\mathbf{A}^{(j+1)} \exp\big\{\mathrm{E}^{(j)}[\log(\pi_t)]\\ &-0.5\mathrm{Tr}(\Delta_t^{(j+1)}(\mathbf{R}_1)^{-1})\big\}\end{aligned} \tag{35}$$

$$\begin{aligned}\mathrm{Pr}^{(j+1)}(\lambda_t = 0) = \ &\mathbf{A}^{(j+1)} \exp\big\{\mathrm{E}^{(j)}[\log(1-\pi_t)]\\ &-0.5\mathrm{Tr}(\mathbf{g}_t{\mathbf{g}_t}^{\mathrm{T}}(\mathbf{R}_1)^{-1})\big\}\end{aligned} \tag{36}$$

where $\mathbf{A}^{(j+1)}$ denotes a constant parameter. Then,

$$\mathrm{E}^{(j+1)}[\lambda_t] = \frac{\mathrm{Pr}^{(j+1)}(\lambda_t = 1)}{\mathrm{Pr}^{(j+1)}(\lambda_t = 1) + \mathrm{Pr}^{(j+1)}(\lambda_t = 0)} \tag{37}$$

Let $\theta = \pi_t$ and from (24), we obtain

$$\begin{aligned}&\log q^{(j+1)}(\pi_t)\\ \propto\ &\mathrm{E}^{(j+1)}[\lambda_t]\log\pi_t + (1-\mathrm{E}^{(j+1)}[\lambda_t])\log(1-\pi_t)\\ &+(a_0-1)\log\pi_t + (b_0-1)\log(1-\pi_t) + c_{\pi_t}\end{aligned} \tag{38}$$

$q^{(j+1)}(\pi_t)$ is approximated by a Beta distribution,

$$q^{(j+1)}(\pi_t) = \mathrm{Be}(\pi_t; a_t^{(j+1)}, b_t^{(j+1)}) \tag{39}$$

where $a_t^{(j+1)}$ and $b_t^{(j+1)}$ are given as

$$a_t^{(j+1)} = a_0 + \mathrm{E}^{(j+1)}[\lambda_t] \tag{40}$$

$$b_t^{(j+1)} = b_0 + 1 - \mathrm{E}^{(j+1)}[\lambda_t] \tag{41}$$

Therefore, we obtain

$$\mathrm{E}^{(j+1)}[\log\pi_t] = \phi(a_t^{(j+1)}) - \phi(a_t^{(j+1)} + b_t^{(j+1)}) \tag{42}$$

$$\mathrm{E}^{(j+1)}[\log(1-\pi_t)] = \phi(b_t^{(j+1)}) - \phi(a_t^{(j+1)} + b_t^{(j+1)}) \tag{43}$$

where $\phi(.)$ is the digamma function [30].

Let $\theta = \varepsilon_t$ and from (24), we obtain

$$\begin{aligned}&\log q^{(j+1)}(\varepsilon_t)\\ \propto\ &-0.5\varepsilon_t \mathrm{Tr}(\Pi_t^{(j+1)}(\mathbf{R}_2)^{-1}) - 0.5(1-\varepsilon_t)\mathrm{Tr}(\mathbf{m}_t{\mathbf{m}_t}^{\mathrm{T}}(\mathbf{R}_2)^{-1})\\ &+\varepsilon_t \mathrm{E}^{(j)}[\log(\alpha_t)] + (1-\varepsilon_t)\mathrm{E}^{(j)}[\log(1-\alpha_t)] + c_{\varepsilon_t}\end{aligned} \tag{44}$$

where $\Pi_t^{(j+1)}$ is

$$\begin{aligned}&\Pi_t^{(j+1)}\\ =\ &\mathrm{E}^{(j+1)}\left[(\mathbf{m}_t - \mathbf{C}_2\mathbf{x}_t)(\mathbf{m}_t - \mathbf{C}_2\mathbf{x}_t)^{\mathrm{T}}\right]\\ =\ &(\mathbf{m}_t - \mathbf{C}_2\hat{\mathbf{x}}_{t|t}^{(j+1)})(\mathbf{m}_t - \mathbf{C}_2\hat{\mathbf{x}}_{t|t}^{(j+1)})^{\mathrm{T}} + \mathbf{C}_2\mathbf{P}_{t|t}^{(j+1)}{\mathbf{C}_2}^{\mathrm{T}}\end{aligned} \tag{45}$$

$q^{(j+1)}(\varepsilon_t)$ is approximated by a Bernoulli distribution, we obtain

$$\begin{aligned}\mathrm{Pr}^{(j+1)}(\varepsilon_t = 1) = \ &\mathbf{B}^{(j+1)} \exp\big\{\mathrm{E}^{(j)}[\log(\varepsilon_t)]\\ &-0.5\mathrm{Tr}(\Pi_t^{(j+1)}(\mathbf{R}_2)^{-1})\big\}\end{aligned} \tag{46}$$

$$\begin{aligned}\mathrm{Pr}^{(j+1)}(\varepsilon_t = 0) = \ &\mathbf{B}^{(j+1)} \exp\big\{\mathrm{E}^{(j)}[\log(1-\varepsilon_t)]\\ &-0.5\mathrm{Tr}(\mathbf{m}_t{\mathbf{m}_t}^{\mathrm{T}}(\mathbf{R}_2)^{-1})\big\}\end{aligned} \tag{47}$$

where $\mathbf{B}^{(j+1)}$ denotes a constant parameter. Then,

$$\mathrm{E}^{(j+1)}[\varepsilon_t] = \frac{\mathrm{Pr}^{(j+1)}(\varepsilon_t = 1)}{\mathrm{Pr}^{(j+1)}(\varepsilon_t = 1) + \mathrm{Pr}^{(j+1)}(\varepsilon_t = 0)} \tag{48}$$

Let $\theta = \alpha_t$ and from (24), we obtain

$$\begin{aligned}&\log q^{(j+1)}(\alpha_t)\\ \propto\ &\mathrm{E}^{(j+1)}[\varepsilon_t]\log\alpha_t + (1-\mathrm{E}^{(j+1)}[\varepsilon_t])\log(1-\alpha_t)\\ &+(h_0-1)\log\alpha_t + (d_0-1)\log(1-\alpha_t) + c_{\alpha_t}\end{aligned} \tag{49}$$

$q^{(j+1)}(\alpha_t)$ is approximated by a Beta distribution,

$$q^{(j+1)}(\alpha_t) = \mathrm{Be}(\alpha_t; h_t^{(j+1)}, d_t^{(j+1)}) \tag{50}$$

where $h_t^{(j+1)}$ and $d_t^{(j+1)}$ are

$$h_t^{(j+1)} = h_0 + \mathrm{E}^{(j+1)}[\varepsilon_t] \tag{51}$$

$$d_t^{(j+1)} = d_0 + 1 - \mathrm{E}^{(j+1)}[\varepsilon_t] \tag{52}$$

Therefore, we obtain

$$\mathrm{E}^{(j+1)}[\log\alpha_t] = \phi(h_t^{(j+1)}) - \phi(h_t^{(j+1)} + d_t^{(j+1)}) \tag{53}$$

$$\mathrm{E}^{(j+1)}[\log(1-\alpha_t)] = \phi(d_t^{(j+1)}) - \phi(h_t^{(j+1)} + d_t^{(j+1)}) \tag{54}$$

Let $\theta = \delta_t$ and from (24), we obtain

$$\begin{aligned}&\log q^{(j+1)}(\delta_t)\\ \propto\ &-0.5\delta_t \mathrm{Tr}(\Upsilon_t^{(j+1)}(\mathbf{R}_3)^{-1}) - 0.5(1-\delta_t)\mathrm{Tr}(\mathbf{L}_t{\mathbf{L}_t}^{\mathrm{T}}(\mathbf{R}_3)^{-1})\\ &+\delta_t \mathrm{E}^{(j)}[\log(\beta_t)] + (1-\delta_t)\mathrm{E}^{(j)}[\log(1-\beta_t)] + c_{\delta_t}\end{aligned} \tag{55}$$

where $\Upsilon_t^{(j+1)}$ is

$$\begin{aligned}&\Upsilon_t^{(j+1)}\\ =\ &\mathrm{E}^{(j+1)}\left[(\mathbf{L}_t - \mathbf{C}_3\mathbf{x}_t)(\mathbf{L}_t - \mathbf{C}_3\mathbf{x}_t)^{\mathrm{T}}\right]\\ =\ &(\mathbf{L}_t - \mathbf{C}_3\hat{\mathbf{x}}_{t|t}^{(j+1)})(\mathbf{L}_t - \mathbf{C}_3\hat{\mathbf{x}}_{t|t}^{(j+1)})^{\mathrm{T}} + \mathbf{C}_3\mathbf{P}_{t|t}^{(j+1)}{\mathbf{C}_3}^{\mathrm{T}}\end{aligned} \tag{56}$$

$q^{(j+1)}(\delta_t)$ is approximated by a Bernoulli distribution,

$$\begin{aligned}\mathrm{Pr}^{(j+1)}(\delta_t = 1) = \ &\mathbf{D}^{(j+1)} \exp\big\{\mathrm{E}^{(j)}[\log(\beta_t)]\\ &-0.5\mathrm{Tr}(\Upsilon_t^{(j+1)}(\mathbf{R}_3)^{-1})\big\}\end{aligned} \tag{57}$$

$$\begin{aligned}\mathrm{Pr}^{(j+1)}(\delta_t = 0) = \ &\mathbf{D}^{(j+1)} \exp\big\{\mathrm{E}^{(j)}[\log(1-\beta_t)]\\ &-0.5\mathrm{Tr}(\mathbf{L}_t{\mathbf{L}_t}^{\mathrm{T}}(\mathbf{R}_3)^{-1})\big\}\end{aligned} \tag{58}$$

where $\mathbf{D}^{(j+1)}$ is a constant parameter. Then,

$$\mathrm{E}^{(j+1)}[\delta_t] = \frac{\mathrm{Pr}^{(j+1)}(\delta_t = 1)}{\mathrm{Pr}^{(j+1)}(\delta_t = 1) + \mathrm{Pr}^{(j+1)}(\delta_t = 0)} \tag{59}$$

Let $\theta = \beta_t$ and from (24), we obtain

$$\begin{aligned}&\log q^{(j+1)}(\beta_t)\\ \propto\ &\mathrm{E}^{(j+1)}[\delta_t]\log\beta_t + (1-\mathrm{E}^{(j+1)}[\delta_t])\log(1-\beta_t)\\ &+(e_0-1)\log\beta_t + (f_0-1)\log(1-\beta_t) + c_{\beta_t}\end{aligned} \tag{60}$$

$q^{(j+1)}(\beta_t)$ is approximated by a Beta distribution,

$$q^{(j+1)}(\beta_t) = \mathrm{Be}(\beta_t; e_t^{(j+1)}, f_t^{(j+1)}) \tag{61}$$

where $e_t^{(j+1)}$ and $f_t^{(j+1)}$ are

$$e_t^{(j+1)} = e_0 + \mathrm{E}^{(j+1)}[\delta_t] \tag{62}$$

$$f_t^{(j+1)} = f_0 + 1 - \mathrm{E}^{(j+1)}[\delta_t] \tag{63}$$

Therefore, we obtain,

$$\mathrm{E}^{(j+1)}[\log\beta_t] = \phi(e_t^{(j+1)}) - \phi(e_t^{(j+1)} + f_t^{(j+1)}) \tag{64}$$

$$\mathrm{E}^{(j+1)}[\log(1-\beta_t)] = \phi(f_t^{(j+1)}) - \phi(e_t^{(j+1)} + f_t^{(j+1)}) \tag{65}$$

The proposed VBASF is shown in **Algorithm** 1, where J stands for the iteration number and η denotes the threshold.

Algorithm 1 The proposed VBASF method

Require:

GPS measurement $\mathbf{g}_t$, IMU measurement $\mathbf{m}_t$, Lidar measurement $\mathbf{L}_t$, IV's state mean $\hat{\mathbf{x}}_{t-1|t-1}$ and covariance $\mathbf{P}_{t-1|t-1}$, $\mathbf{C_1}$, $\mathbf{C_2}$, $\mathbf{C_3}$, covariances $\mathbf{Q}$, $\mathbf{R_1}$, $\mathbf{R_2}$, and $\mathbf{R_3}$, a_0, b_0, h_0, d_0, e_0, f_0, η, J

1: Letting $\mathrm{E}^{(0)}[\lambda_t] = \mathrm{E}^{(0)}[\varepsilon_t] = \mathrm{E}^{(0)}[\delta_t] = 1$, $\mathrm{E}^{(0)}[\log\pi_t] = \phi(a_0) - \phi(a_0+b_0)$, $\mathrm{E}^{(0)}[\log(1-\pi_t)] = \phi(b_0) - \phi(a_0+b_0)$, $\mathrm{E}^{(0)}[\log\alpha_t] = \phi(h_0) - \phi(h_0+d_0)$, $\mathrm{E}^{(0)}[\log(1-\alpha_t)] = \phi(d_0) - \phi(h_0+d_0)$, $\mathrm{E}^{(0)}[\log\beta_t] = \phi(e_0) - \phi(e_0+f_0)$, $\mathrm{E}^{(0)}[\log(1-\beta_t)] = \phi(f_0) - \phi(e_0+f_0)$.

2: **for** $j = 0 : J-1$ **do**

3: Calculate $\hat{\mathbf{x}}_{t|t}^{(j+1)}$ and $\mathbf{P}_{t|t}^{(j+1)}$ using (30) and (31), respectively

4: If $\frac{\left\| \hat{\mathbf{x}}_{t|t}{}^{(j+1)} - \hat{\mathbf{x}}_{t|t}{}^{(j)} \right\|}{\left\| \hat{\mathbf{x}}_{t|t}{}^{(j+1)} \right\|} \leq \eta$, terminate iteration

5: Compute $\mathrm{E}^{(l+1)}[\lambda_t]$ as in (37)

6: Compute $\mathrm{E}^{(l+1)}[\pi_t]$ and $\mathrm{E}^{(j+1)}[\log(1-\pi_t)]$ using (42) and (43), respectively

7: Compute $\mathrm{E}^{(j+1)}[\varepsilon_t]$ using (48)

8: Compute $\mathrm{E}^{(j+1)}[\alpha_t]$ and $\mathrm{E}^{(j+1)}[\log(1-\alpha_t)]$ using (53) and (54), respectively

9: Compute $\mathrm{E}^{(j+1)}[\delta_t]$ using (59)

10: Compute $\mathrm{E}^{(j+1)}[\beta_t]$ and $\mathrm{E}^{(j+1)}[\log(1-\beta_t)]$ using (64) and (65), respectively

11: **end for**

12: $\hat{\mathbf{x}}_{t|t} = \hat{\mathbf{x}}_{t|t}^{(J)}$, $\mathbf{P}_{t|t} = \mathbf{P}_{t|t}^{(J)}$

Ensure:

$\hat{\mathbf{x}}_{t|t}$, $\mathbf{P}_{t|t}$

In this article, the parameters λ_t, ε_t, and δ_t recognize whether the GPS, IMU, and Lidar measurements have the useful information to improve the localization performance. When λ_t=1, ε_t=1, and δ_t=1, it means that every measurements are fused.

Proposition 1: If the prior parameters a_0, b_0, h_0, d_0, e_0, and f_0 are chosen as $a_0 = h_0 = e_0 = 1$ and $b_0 = d_0 = f_0 = 0$, the proposed VBASF becomes EKF with augmented measurements.

Proof: Proposition 1 is proved by mathematical induction. For j=0, let

$$\mathrm{E}^{(0)}[\lambda_t] = 1, \mathrm{E}^{(0)}[\varepsilon_t] = 1, \mathrm{E}^{(0)}[\delta_t] = 1 \tag{66}$$

$$\begin{aligned}\mathrm{E}^{(0)}[\log(\pi_t)] &= \phi(a_0) - \phi(a_0+b_0)\\ &= \phi(1) - \phi(1) = 0\end{aligned} \tag{67}$$

$$\begin{aligned}\mathrm{E}^{(0)}[\log(1-\pi_t)] &= \phi(b_0) - \phi(a_0+b_0)\\ &= \phi(0) - \phi(1) = -\infty\end{aligned} \tag{68}$$

$$\begin{aligned}\mathrm{E}^{(0)}[\log\alpha_t] &= \phi(h_0) - \phi(h_0+d_0)\\ &= \phi(1) - \phi(1) = 0\end{aligned} \tag{69}$$

$$\begin{aligned}\mathrm{E}^{(0)}[\log(1-\alpha_t)] &= \phi(d_0) - \phi(h_0+d_0)\\ &= \phi(0) - \phi(1) = -\infty\end{aligned} \tag{70}$$

$$\begin{aligned}\mathrm{E}^{(0)}[\log\beta_t] &= \phi(e_0) - \phi(e_0+f_0)\\ &= \phi(1) - \phi(1) = 0\end{aligned} \tag{71}$$

$$\begin{aligned}\mathrm{E}^{(0)}[\log(1-\beta_t)] &= \phi(f_0) - \phi(e_0+f_0)\\ &= \phi(0) - \phi(1) = -\infty\end{aligned} \tag{72}$$

Substituting (66) into (29), we have

$$\bar{\mathbf{R}}_t^{(0)} = \begin{bmatrix} \mathbf{R}_1 & \mathbf{0} & \mathbf{0} \\ \mathbf{0} & \mathbf{R}_2 & \mathbf{0} \\ \mathbf{0} & \mathbf{0} & \mathbf{R}_3 \end{bmatrix} \tag{73}$$

If (66)-(73) hold at the jth iteration, we obtain

$$\mathrm{E}^{(j)}[\lambda_t] = 1, \mathrm{E}^{(j)}[\varepsilon_t] = 1, \mathrm{E}^{(j)}[\delta_t] = 1 \tag{74}$$

$$\mathrm{E}^{(j)}[\log\pi_t] = 0 \tag{75}$$

$$\mathrm{E}^{(j)}[\log(1-\pi_t)] = -\infty \tag{76}$$

$$\mathrm{E}^{(j)}[\log\alpha_t] = 0 \tag{77}$$

$$\mathrm{E}^{(j)}[\log(1-\alpha_t)] = -\infty \tag{78}$$

$$\mathrm{E}^{(j)}[\log\beta_t] = 0 \tag{79}$$

$$\mathrm{E}^{(j)}[\log(1-\beta_t)] = -\infty \tag{80}$$

Substituting (75), (76) into (35)-(36), (77), (78) into (46)-(47), (79), (80) into (57)-(58), we have

$$\mathrm{Pr}^{(j+1)}(\lambda_t = 1) = \mathbf{A}^{(j+1)} \exp\{-0.5\mathrm{Tr}(\Delta_t^{(j+1)}(\mathbf{R}_1)^{-1})\} \tag{81}$$

$$\mathrm{Pr}^{(j+1)}(\lambda_t = 0) = 0 \tag{82}$$

$$\mathrm{Pr}^{(j+1)}(\varepsilon_t = 1) = \mathbf{B}^{(j+1)} \exp\{-0.5\mathrm{Tr}(\Pi_t^{(j+1)}(\mathbf{R}_2)^{-1})\} \tag{83}$$

$$\mathrm{Pr}^{(j+1)}(\varepsilon_t = 0) = 0 \tag{84}$$

$$\mathrm{Pr}^{(j+1)}(\delta_t = 1) = \mathbf{D}^{(j+1)} \exp\{-0.5\mathrm{Tr}(\Upsilon_t^{(j+1)}(\mathbf{R}_3)^{-1})\} \tag{85}$$

$$\mathrm{Pr}^{(j+1)}(\delta_t = 0) = 0 \tag{86}$$

Substituting (81), (82) into (37), (83), (84) into (48), (85), (86) into (59), we have

$$\mathrm{E}^{(j+1)}[\lambda_t] = 1, \mathrm{E}^{(j+1)}[\varepsilon_t] = 1, \mathrm{E}^{(j+1)}[\delta_t] = 1 \tag{87}$$

Using (87) into (29), we have

$$\bar{\mathbf{R}}_t^{(j+1)} = \begin{bmatrix} \mathbf{R}_1 & \mathbf{0} & \mathbf{0} \\ \mathbf{0} & \mathbf{R}_2 & \mathbf{0} \\ \mathbf{0} & \mathbf{0} & \mathbf{R}_3 \end{bmatrix} \tag{88}$$

From the above induction, the noise covariance $\bar{\mathbf{R}}_t^{(j+1)}$ of the proposed method at every time t for each iteration is equal to that of EKF with augmented measurements. Therefore, the proposed VBASF becomes EKF with augmented measurements when $a_0 = h_0 = e_0 = 1$ and $b_0 = d_0 = f_0 = 0$. ■

In this paper, the optimal solution of state estimation for IV with multiple sensors is proposed by a novel fusion method, which introduces an indicator to identify whether the measurement has the useful information for improving the localization accuracy of IV.

IV. Experiments

The performance of the proposed VBASF method for estimating the IV's state is verified by simulations and real IV experiments.

A. Simulations

The motions of IV and sensor measurements are given by (1), (2), (4), and (7), respectively. The time interval and total time are set as 0.01s and 200s, respectively. The covariance $\mathbf{Q}$ is set as $diag(10^{-2}\mathbf{I}_3\text{m}^2, 10^{-6}\mathbf{I}_3\text{rad}^2, 10^{-2}\mathbf{I}_3 {}^{\text{m}^2}/_{\text{s}^2}, 10^{-6}\mathbf{I}_3 {}^{\text{rad}^2}/_{\text{s}^2})$, $\mathbf{R}_1 = diag(a_1\mathbf{I}_3)$, $\mathbf{R}_2 = diag(a_2\mathbf{I}_3)$, and $\mathbf{R}_3 = diag(a_3\mathbf{I}_3, a_4\mathbf{I}_3)$, where $a_1 = 10\text{m}^2$, $a_2 = 0.1 {}^{\text{rad}^2}/_{\text{s}^2}$, $a_3 = 1 {}^{\text{m}^2}/_{\text{s}^2}$, and $a_4 = 1 {}^{\text{rad}^2}/_{\text{s}^2}$. In order to describe the GPS measurement loss, Lidar and IMU measurements outlier, we set 10 percents of GPS, IMU, and Lidar measurements as useless information.

In this paper, BKF-MAP method [9], BKF-CML method [9] method, and the KF with true measurement (KFT) method are compared. The KFT uses the true measurement to provide optimal state estimates. The BKF-MAP method is computed under the criterion of maximum a posteriori probability. The conditional measurement loss probability is estimated in the BKF-CML method [9]. In the proposed VBASF method, we set a_0=h_0=e_0=0.85, b_0=d_0=f_0=0.15, η=0.01, J=20. In this paper, the performance indices are given as:

$$\text{RMSE}_\text{p} = \sqrt{\frac{\sum_{i=1}^{MC}\left((p_t^{x,i} - \hat{p}_t^{x,i})^2 + (p_t^{y,i} - \hat{p}_t^{y,i})^2 + (p_t^{z,i} - \hat{p}_t^{z,i})^2\right)}{MC}} \quad (89)$$

$$\text{RMSE}_\text{o} = \sqrt{\frac{\sum_{i=1}^{MC}\left((\phi_t^i - \hat{\phi}_t^i)^2 + (\theta_t^i - \hat{\theta}_t^i)^2 + (\psi_t^i - \hat{\psi}_t^i)^2\right)}{MC}} \quad (90)$$

where RMSE_p and RMSE_o denote the root mean square error of position and orientation, respectively, MC is the total number, $(p_t^{x,i}, p_t^{y,i}, p_t^{z,i})$ and $(\phi_t^i, \theta_t^i, \psi_t^i)$ denote the true positions and orientation at time t in the ith run, respectively, $(\hat{p}_t^{x,i}, \hat{p}_t^{y,i}, \hat{p}_t^{z,i})$ and $(\hat{\phi}_t^i, \hat{\theta}_t^i, \hat{\psi}_t^i)$ denote the estimated positions and orientation at the ith run at time t, respectively. The initial state estimate is chosen as $\mathcal{N}(\mathbf{x}_0, P_0)$, where $\mathbf{x}_0 = \mathbf{0}$ and $P_0 = \mathbf{I}_{12}$.

Using 100 runs, Fig. 1 and Fig. 2 depict the RMSE_p and RMSE_o of the BKF-MAP, BKF-CML, KFT, and proposed VBASF methods, respectively. From Fig. 1 and Fig. 2, the proposed VBASF method has smaller RMSE_p and RMSE_o than the BKF-MAP and BKF-CML methods, the RMSE_p and RMSE_o of proposed VBASF method are close to those of KFT method.

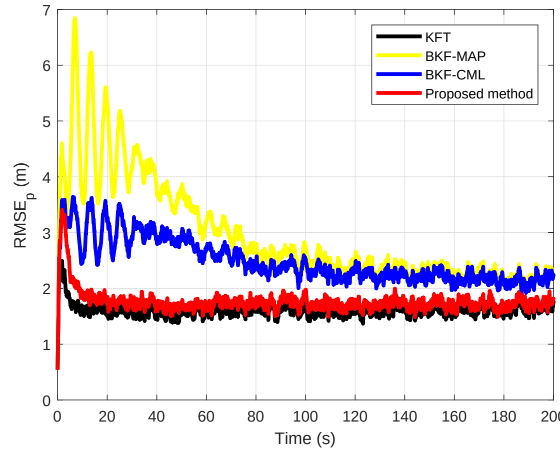

Fig. 1. $\mathbf{RMSE_p}$ of the BKF-MAP, BKF-CML, KFT, and proposed VBASF method

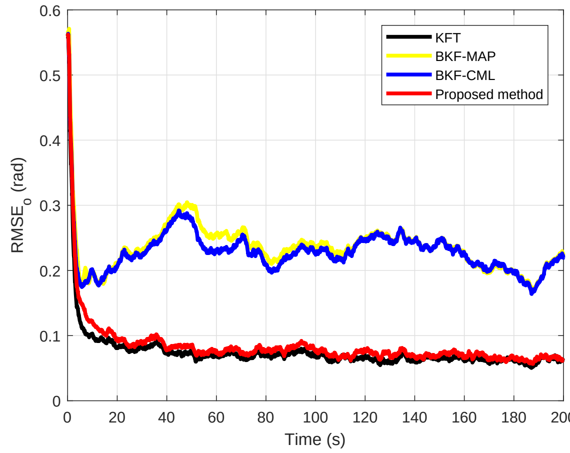

Fig. 2. $\mathbf{RMSE_o}$ of the BKF-MAP, BKF-CML, KFT, and proposed VBASF method

B. Field experiment

Real IV experiments are conducted in this subsection. An IMU, a Velodyne Lidar-32, and a low-precision GPS are equipped on the IV. Meanwhile, a integrated navigation system (INS), which provides the reference trajectory of the IV, is also equipped on the IV. Fig. 3 and Fig. 4 give the real IV and experimental route, respectively.

The measurements in (2) and (4) are obtained from the information of the low-precision GPS and the IMU. The ICP algorithm [27] is proposed to give the measurement in (6), which is computed from Lidar point set. The measurements of GPS and reference trajectory are given in Fig. 5. It is observed that the GPS measurements are distributed around the reference trajectory. The GPS measurements are highly

Fig. 3. The used IV

Fig. 4. The experimental route

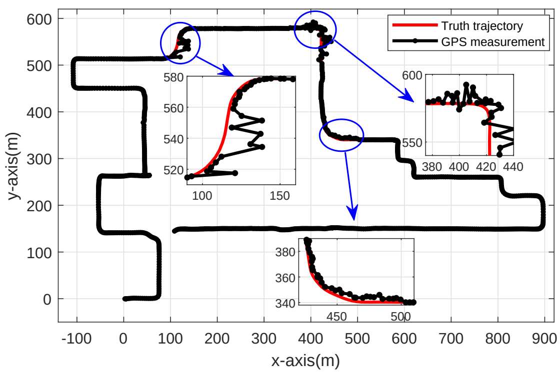

Fig. 5. Truth trajectory and GPS measurement

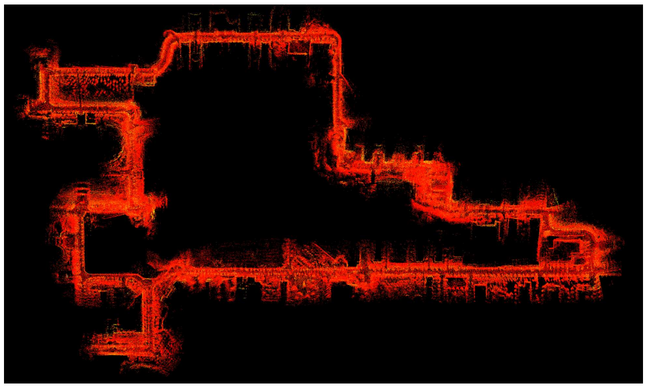

Fig. 6. Map built by the proposed VBASF method

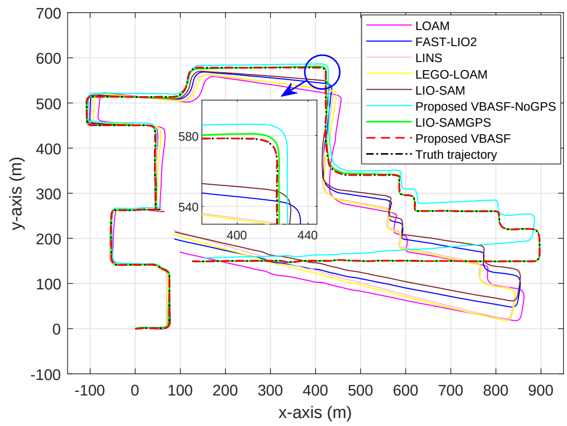

Fig. 7. Truth and estimated trajectories

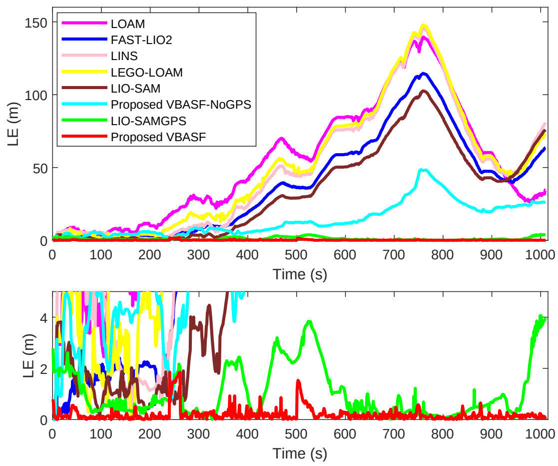

Fig. 8. LEs of these compared methods, proposed VBASF-NoGPS method, and proposed VBASF method

contaminated with outliers over time periods 350-400 s, 440-480 s, and 515-555 s. Meanwhile, to exhibit the robustness of the proposed method, some difficult scenarios are manually added, such as, the maximum Lidar sensing distance is restricted within 10m over time periods 200-220 s, 310-325 s, and 535-550 s.

In the experiments, the covariance of process noise and three sensor measurement noises are set as identity matrices, respectively. Using the proposed VBASF method, the IV's state is estimated. The map is produced by the proposed VBASF method in Fig. 6. It can be seen that the map matches well with the ground truths.

To evaluate the proposed VBASF method, several traditional Lidar-SLAM methods are compared, such as LOAM method [18], FAST-LIO2 method [24], LINS method [25], LEGO-LOAM method [19], LIO-SAM method [31]. In the LOAM method, IV's state is estimated by point cloud registration algorithm. In the FAST-LIO2 method, Lidar-inertial odometry is performed by an iterated KF. In the LINS method, an iterated error-state KF is developed to obtain the IV's state using Lidar and IMU. LEGO-LOAM method uses Levenberg-Marquardt optimization algorithm to obtain the IV's state. LIO-SAM fuses Lidar and IMU measurements to obtain Lidar inertial odometry in a factor graph. The LIO-SAMGPS method, which fuses GPS, Lidar, and IMU in the framework of LIO-SAM, is compared. Furthermore, the proposed VBASF-NoGPS, which uses the proposed VBASF without GPS measurements, is also considered. The estimated trajectories of the compared methods, proposed VBASF-NoGPS method, and proposed VBASF are given in Fig. 7. It is shown that the trajectories from VBASF is close to the ground truths.

The localization error (LE) is chosen as the performance index,

$$\mathrm{LE} = \sqrt{(x_t^{IV} - \hat{x}_t^{IV})^2 + (y_t^{IV} - \hat{y}_t^{IV})^2 + (z_t^{IV} - \hat{z}_t^{IV})^2} \tag{91}$$

where $(\hat{x}_t^{IV}, \hat{y}_t^{IV}, \hat{z}_t^{IV})$ and $(x_t^{IV}, y_t^{IV}, z_t^{IV})$ denote the estimated and true positions of IV, respectively.

The LEs of the LOAM method, FAST-LIO2 method, LINS method, LEGO-LOAM method, LIO-SAM method, LIO-SAMGPS method, proposed VBASF-NoGPS method, and proposed VBASF method are shown in Fig. 8. The proposed VBASF method has smaller LE than other methods. The proposed VBASF-NoGPS method has better performance than the LOAM method, FAST-LIO2 method, LINS method, LEGO-LOAM method and LIO-SAM method. In the experiments, the GPS measurements are highly contaminated with outliers over time periods 350-400 s, 440-480 s, and 515-555 s. The geometric features of Lidar are scarce over time periods 200-220 s, 310-325 s, and 535-550 s. The LIO-SAMGPS method directly fuses the measurements of all sensors to localize the IV, and it is sensitive to outliers. The proposed VBASF method fuses only useful sensor measurements and has better performance than LIO-SAMGPS method. Meanwhile, the proposed VBASF-NoGPS method also fuses only useful sensor measurements and outperforms the LOAM method, FAST-LIO2 method, LINS method, LEGO-LOAM method, LIO-SAM method. The run times in one step of these methods are listed in Table. I, which reveals that the proposed VBASF has lower computation load than the LOAM, LEGO-LOAM, LIO-SAM, LINS, and LIO-SAMGPS methods, and it has slightly higher computational load than the FAST-LIO2 method.

TABLE I
THE RUN-TIMES OF THE LOAM, FAST-LIO2, LINS, LEGO-LOAM, LIO-SAM, LIO-SAMGPS, PROPOSED VBASF-NOGPS AND PROPOSED VBASF METHODS

Methods	Run-time (ms)
LOAM	78.26
FAST-LIO2	30.82
LINS	168.56
LEGO-LOAM	50.75
LIO-SAM	70.55
LIO-SAMGPS	125.45
Proposed VBASF-NoGPS	33.9
Proposed VBASF	40.2

V. CONCLUSIONS

In this study, a novel VBASF method is proposed to localize IV. An indicator, which follows a Bernoulli distribution, is used to identify whether the sensor measurement has useful information to improve the localization performance. The VB algorithm is proposed to provide the robust localization results. Simulations and real IV experiments are performed to compare the proposed VBASF method and the existing state-of-the-art methods. It can be concluded that the proposed VBASF method has improved localization accuracy than the LOAM, FAST-LIO2, LINS, LEGO-LOAM, LIO-SAM, and LIO-SAMGPS methods but has slightly higher computational load than the FAST-LIO2 method.

REFERENCES

[1] H. Zhu, K. Yuen, L. Mihaylova, and H. Leung, "Overview of environment perception for intelligent vehicles," *IEEE Transactions on Intelligent Transportation Systems*, vol. 18, no. 10, pp. 2584–2601, 2017.

[2] Y. Lu, H. Ma, E. Smart, and H. Yu, "Real-time performance-focused localization techniques for autonomous vehicle: A review," *IEEE Transactions on Intelligent Transportation Systems*, vol. 23, no. 7, pp. 6082–6100, 2022.

[3] H. Zhu, J. Mi, Y. Li, K.-V. Yuen, and H. Leung, "VB-Kalman based localization for connected vehicles with delayed and lost measurements: Theory and experiments," *IEEE/ASME Transactions on Mechatronics*, vol. 27, no. 3, pp. 1370–1378, 2022.

[4] B. Farina, J. Toledo, and L. Acosta, "Augmented Kalman filter design in a localization system using onboard sensors with intrinsic delays," *IEEE Sensors Journal*, vol. 23, no. 11, pp. 12 105–12 113, 2023.

[5] M. Brossard, A. Barrau, and S. Bonnabel, "AI-IMU dead-reckoning," *IEEE Transactions on Intelligent Vehicles*, vol. 5, no. 4, pp. 585–595, 2020.

[6] W. Liu, D. Caruso, E. Ilg, J. Dong, A. I. Mourikis, K. Daniilidis, V. Kumar, and J. Engel, "TLIO: Tight learned inertial odometry," *IEEE Robotics and Automation Letters*, vol. 5, no. 4, pp. 5653–5660, 2020.

[7] R. Arnay, J. Hernndez-Aceituno, J. Toledo, and L. Acosta, "Laser and optical flow fusion for a non-intrusive obstacle detection system on an intelligent wheelchair," *IEEE Sensors Journal*, vol. 18, no. 9, pp. 3799–3805, 2018.

[8] D. Perea-Strom, A. Morell, J. Toledo, and L. Acosta, "GNSS integration in the localization system of an autonomous vehicle based on particle weighting," *IEEE Sensors Journal*, vol. 20, no. 6, pp. 3314–3323, 2020.

[9] J. Zhang, K. You, and L. Xie, "Bayesian filtering with unknown sensor measurement losses," *IEEE Transactions on Control of Network Systems*, vol. 6, no. 1, pp. 163–175, 2019.

[10] A. Chalvatzaras, I. Pratikakis, and A. A. Amanatiadis, "A survey on map-based localization techniques for autonomous vehicles," *IEEE Transactions on Intelligent Vehicles*, pp. 1–23, 2022.

[11] C. Cadena, L. Carlone, H. Carrillo, Y. Latif, D. Scaramuzza, J. Neira, I. Reid, and J. J. Leonard, "Past, present, and future of simultaneous localization and mapping: Toward the robust-perception age," *IEEE Transactions on Robotics*, vol. 32, no. 6, pp. 1309–1332, 2016.

[12] G. Bresson, Z. Alsayed, L. Yu, and S. Glaser, "Simultaneous localization and mapping: A survey of current trends in autonomous driving," *IEEE Transactions on Intelligent Vehicles*, vol. 2, no. 3, pp. 194–220, 2017.

[13] H. Xing, Y. Liu, S. Guo, L. Shi, X. Hou, W. Liu, and Y. Zhao, "A multi-sensor fusion self-localization system of a miniature underwater robot in structured and GPS-denied environments," *IEEE Sensors Journal*, vol. 21, no. 23, pp. 27 136–27 146, 2021.

[14] Y. Wang, Y. Lou, W. Song, Z. Tu, Y. Wang, and S. Zhang, "Simultaneous localization of rail vehicles and mapping of surroundings with LiDAR-inertial-GNSS integration," *IEEE Sensors Journal*, vol. 22, no. 14, pp. 14 501–14 512, 2022.

[15] S. Kuutti, S. Fallah, K. Katsaros, M. Dianati, F. Mccullough, and A. Mouzakitis, "A survey of the state-of-the-art localization techniques and their potentials for autonomous vehicle applications," *IEEE Internet of Things Journal*, vol. 5, no. 2, pp. 829–846, 2018.

[16] Q. Zou, Q. Sun, L. Chen, B. Nie, and Q. Li, "A comparative analysis of LiDAR SLAM-based indoor navigation for autonomous vehicles," *IEEE Transactions on Intelligent Transportation Systems*, vol. 23, no. 7, pp. 6907–6921, 2022.

[17] S. Chen, H. Ma, C. Jiang, B. Zhou, W. Xue, Z. Xiao, and Q. Li, "NDT-LOAM: A real-time lidar odometry and mapping with weighted NDT and LFA," *IEEE Sensors Journal*, vol. 22, no. 4, pp. 3660–3671, 2021.

[18] J. Zhang and S. Singh, "LOAM: LiDAR odometry and mapping in real time," in *Proceedings of Robotics: Science and Systems*, 2014, pp. 1–9.

[19] T. Shan and B. Englot, "LeGO-LOAM: Lightweight and ground-optimized Lidar odometry and mapping on variable terrain," in *2018 IEEE/RSJ International Conference on Intelligent Robots and Systems (IROS)*, 2018, pp. 4758–4765.

[20] J. Zhang and S. Singh, "Low-drift and real-time Lidar odometry and mapping," *Autonomous Robots*, vol. 41, no. 2, pp. 401–416, 2017.

[21] Y. Wu, Y. Li, W. Li, H. Li, and R. Lu, "Robust Lidar-based localization scheme for unmanned ground vehicle via multisensor fusion," *IEEE Transactions on Neural Networks and Learning Systems*, vol. 32, no. 12, pp. 5633–5643, 2021.

[22] Z. Wu, D. Yuan, F. Zhang, and M. Yao, "Low-cost attitude estimation using GPS/IMU fusion aided by land vehicle model constraints and gravity-based angles," *IEEE Transactions on Intelligent Transportation Systems*, vol. 23, no. 8, pp. 13 386–13 402, 2022.

[23] H. Zhu, Q. Wang, Y. Li, and H. Leung, "Variational Bayesian based localization for intelligent vehicle using lidar and GPS data fusion: Algorithm and experiments," *IEEE/ASME Transactions on Mechatronics*, pp. 1–9, 2022.

[24] W. Xu, Y. Cai, D. He, J. Lin, and F. Zhang, "FAST-LIO2: Fast direct Lidar-inertial odometry," *IEEE Transactions on Robotics*, vol. 38, no. 4, pp. 2053–2073, 2022.

[25] C. Qin, H. Ye, C. E. Pranata, J. Han, S. Zhang, and M. Liu, "LINS: A Lidar-inertial state estimator for robust and efficient navigation," in *2020 IEEE International Conference on Robotics and Automation (ICRA)*, 2020, pp. 8899–8906.

[26] G. P. C. Jnior, A. M. C. Rezende, V. R. F. Miranda, R. Fernandes, H. Azprua, A. A. Neto, G. Pessin, and G. M. Freitas, "EKF-LOAM: An adaptive fusion of LiDAR SLAM with wheel odometry and inertial data for confined spaces with few geometric features," *IEEE Transactions on Automation Science and Engineering*, vol. 19, no. 3, pp. 1458–1471, 2022.

[27] P. Besl and N. D. McKay, "A method for registration of 3-D shapes," *IEEE Transactions on Pattern Analysis and Machine Intelligence*, vol. 14, no. 2, pp. 239–256, 1992.

[28] S. Sarkka and A. Nummenmaa, "Recursive noise adaptive Kalman filtering by variational Bayesian approximations," *IEEE Transactions on Automatic Control*, vol. 54, no. 3, pp. 596–600, 2009.

[29] H. Zhu, G. Zhang, Y. Li, and H. Leung, "An adaptive Kalman filter with inaccurate noise covariances in the presence of outliers," *IEEE Transactions on Automatic Control*, vol. 67, no. 1, pp. 374–381, 2022.

[30] C. M. Bishop, *Pattern Recognition and Machine Learning*. New York: Springer, 2006.

[31] T. Shan, B. Englot, D. Meyers, W. Wang, C. Ratti, and D. Rus, "LIO-SAM: Tightly-coupled Lidar inertial odometry via smoothing and mapping," in *2020 IEEE/RSJ International Conference on Intelligent Robots and Systems (IROS)*, 2020, pp. 5135–5142.

Hao Zhu (Senior Member, IEEE) received his Ph.D. degree in computer science from Chongqing University, Chongqing, China, in 2012. He is currently a professor of Chongqing University of Posts and Telecommunications, Chongqing, China. His current research interests include intelligent and connected vehicles, information fusion, target tracking, and signal processing. Dr. Zhu has authored or co-authored nearly 100 papers. He serves as Associate Editors for the Elsevier Signal Processing Journal and International Journal of Advanced Robotic Systems.

Yujian Qiu received the B.S. degree from the Changshu Institute of Technology, Jiangsu, China, in 2021. He is currently pursuing the M.S. degree in electronic information at Chongqing University of Posts and Telecommunications. His research interests include intelligent and connected vehicles and SLAM.

Yongfu Li (Senior Member, IEEE) received his Ph.D. degree in control science and engineering from Chongqing University, Chongqing, China, in 2012. He is currently a Professor of Chongqing University of Posts and Telecommunications, Chongqing, China. His research interests include intelligent transportation systems and intelligent and connected vehicles.

Lyudmila Mihaylova (Senior Member, IEEE) received her Ph.D. degree in systems and control engineering from the Technical University of Sofia, Bulgaria, in 1996. She is currently a Professor of Signal Processing and Control with the Department of Automatic Control and Systems Engineering, University of Sheffield, Sheffield, United Kingdom. Her research is in the areas of autonomous systems and machine learning with various applications such as navigation, surveillance, and sensor networks. She is Associate Editor-in-Chief for the IEEE Transactions on Aerospace and Electronic Systems since 2021 and a Subject Area Editor for the Elsevier Signal Processing Journal since 2022. She was the president of the International Society of Information Fusion (ISIF) from 2016 to 2018. She is on the Board of Directors of ISIF. She has been serving for organising conferences as the general vice chair of UKCI 2022, a program chair for the International Conference on Information Fusion, Fusion 2022, technical chair for Fusion 2021, publicity chair for IEEE MFI 2021 and UKCI 2021. She was the general vice-chair for the International Conference on Information Fusion 2018 (Cambridge, UK), of the IET Data Fusion Target Tracking 2014 and 2012 Conferences, publications chair for ICASSP 2019 (Brighton, UK) and others.

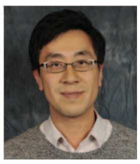

Henry Leung (Fellow, IEEE) received his Ph.D. degree in electrical engineering from McMaster University, Hamilton, ON, Canada, in 1991. He is currently a professor of the University of Calgary, Calgary, AB, Canada. His current research interests include information fusion, robotics, machine learning, signal and image processing, and big data analytic. Dr. Leung has authored or co-authored nearly 500 papers.